

Journal of Materials Chemistry A

Accepted Manuscript



This is an *Accepted Manuscript*, which has been through the Royal Society of Chemistry peer review process and has been accepted for publication.

Accepted Manuscripts are published online shortly after acceptance, before technical editing, formatting and proof reading. Using this free service, authors can make their results available to the community, in citable form, before we publish the edited article. We will replace this *Accepted Manuscript* with the edited and formatted *Advance Article* as soon as it is available.

You can find more information about *Accepted Manuscripts* in the [Information for Authors](#).

Please note that technical editing may introduce minor changes to the text and/or graphics, which may alter content. The journal's standard [Terms & Conditions](#) and the [Ethical guidelines](#) still apply. In no event shall the Royal Society of Chemistry be held responsible for any errors or omissions in this *Accepted Manuscript* or any consequences arising from the use of any information it contains.

Sn- and SnO₂-Graphene Flexible Foams Suitable as Binder-Free Anodes for Lithium Ion Batteries

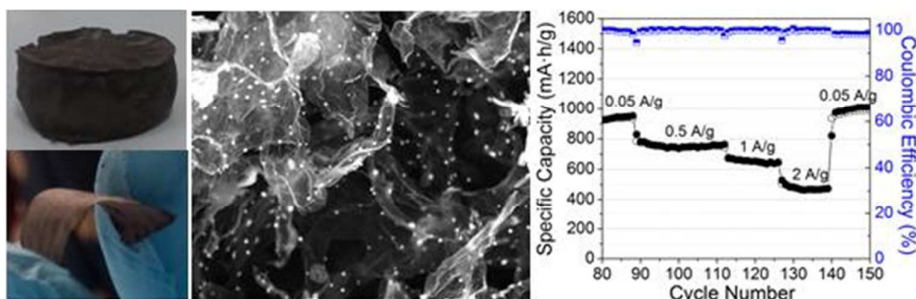
Cristina Botas,^a Daniel Carriazo,*^{a, b} Gurpreet Singh,^a Teófilo Rojo^{a, c}

^a CIC EnergiGUNE, Parque Tecnológico de Álava, Albert Einstein 48, 01510 Miñano, Álava, Spain

^b IKERBASQUE, Basque Foundation for Science, Bilbao, Spain

^c Departamento de Química Inorgánica, Universidad Del País Vasco UPV/EHU, 48080 Bilbao, Spain

Table of contents



A very simple approach for the preparation of flexible free-standing Sn-based graphene composites and its use as binder-free anodes for lithium ion batteries is reported.

Abstract

With the objective of developing new advanced composite materials that can be used as anodes for lithium ion batteries (LIBs), herein we describe the synthesis of a novel three dimensional (3D) macroporous foams formed by reduced graphene oxide (rGO) and submicron tin-based particles. The aerogels were obtained by freeze/freezing-drying a suspension of graphene oxide (GO) in the presence of a tin precursor and its subsequent thermal reduction under argon atmosphere. The materials exhibited a 3D-macroporous structure formed by walls of rGO decorated with Sn or SnO₂ particles depending on the temperature of calcination. Self-standing compressed foams were directly assembled into coin cells without using any metallic support to be evaluated as binder-free anodes for LIBs. The homogeneous dispersion and intimate contact between the Sn-based particles and graphene walls were confirmed by scanning electron microscopy (SEM). The performance of SnO₂-rGO composites materials as anode for LIBs showed larger specific capacity compared with the rGO and metallic Sn-containing samples, reaching in the former case a reversible capacity of 1010 mAh g⁻¹ of electrode at 0.05 A g⁻¹ and good capacity retention (470 mAh g⁻¹) even at 2 A g⁻¹ (~ 2C), among the highest reported for similar systems. SEM images of selected electrodes after 50 charge-discharge cycles

showed that even though SnO₂ submicron particles were pulverized into small nanoparticles it remain intact upon cycling.

Introduction

Lithium ion batteries (LIBs) are the dominant energy storage devices in portable electronics because of its high energy density and low self-discharge rate.^[1] However, the increasing complexity of the portable electronic devices, and the envisioned development of flexible electronics, such as wearable electronics or roll-up displays, require the development of flexible and lightweight materials suitable as electrodes that can store as much energy as possible, and charged as fast as possible.^[2, 3]

Graphite, with a theoretical gravimetric capacity estimated at 372 mAh g⁻¹, is until date the most commonly used material as anode in LIBs because its abundance, good electrical conductivity and low cost. With the aim of improving energy, power and stability of LIBs, new materials have been proposed to replace graphite as anode. Sn or SnO₂ with theoretical reversible specific capacities of 994 and 782 mAh g⁻¹,^[4, 5] respectively, are among the most promising compounds that have been pointed out as alternative anode materials. The main drawback associated to the performance of Sn or SnO₂ as active materials for LIBs is due to its volume change (up to 300%) that occurs upon the lithiation/delithiation process. This extreme increase in the SnO₂ volume can cause the pulverization of the material and/or the growth of an unstable solid electrolyte interface (SEI), which generally leads to low coulombic efficiencies and capacity fading along the cycling.^[6]

To overcome this handicap different strategies such as the use of novel binders or the encapsulation of the Sn-based particles have been proposed.^[7-10] Graphene, an allotrope of carbon consisting of a monolayer of carbon atoms,^[11] with outstanding properties such as flexibility and transparency, electrical conductivity or high specific surface areas, is appointed as a promising material to wrap up or to imbibe the Sn-based particles.^[12] It has been claimed that the presence of graphene not only improves the electronic conductivity of the composites, and therefore its capacity retention at high current rates, but also, graphene sheets can buffer the

volume changes undergone by the Sn-based particles.^[13] Different approaches such as physical mixture of SnO₂ nanoparticles together with graphene sheets^[14] or spray deposition,^[15, 16] have been described for the preparation of these graphene-SnO₂ composites. However, the most explored strategy involves the hydro- or solvo-thermal deposition of very small SnO₂ nanoparticles (generally around 5 nm) on the GO layers,^[17-20] and its subsequent partial reduction by thermal treatments at moderate temperatures under inert atmosphere^[21, 22] or through its reaction with hydrazine.^[23, 24]

On the other hand, graphene macroporous 3D foams showing interesting features namely excellent mechanical strength and high specific surface areas, have been recently evaluated as catalysts, adsorbents or as electrodes for supercapacitor^[25] or LIBs.^[26, 27] However, to the best of our knowledge SnO₂-graphene foams as anodes for LIBs have been scarcely explored.^[22, 24, 28] Recently, Feng *et al.* reported the preparation of SnO₂-graphene by hydrothermal treatment and subsequent chemical reduction with hydrazine showing capacity values of 661 mAh g⁻¹ at 0.5 A g⁻¹ after 60 cycles.^[24] In a posterior work,^[22] the authors tailored the macroporosity of these composites using polymeric templates to obtain highly macroporous scaffolds that were thermally reduced at 450 °C claiming in this later case a specific capacity of 900 mAh g⁻¹ at 0.4 A g⁻¹. In all these works very small SnO₂ nanoparticles (5 nm) on graphene sheets were reported and the materials were grinded to powder to be further processed with conductive carbon in order to improve their electrical conductivity, and a binder (PVDF) for its evaluation as anodes in LIBs.

Herein we present the preparation of flexible macroporous 3D composites formed by reduced graphene oxide and submicron Sn or SnO₂ particles by a very simple route, which involves freeze/freeze-drying a suspension of graphene oxide in the presence of the tin precursor and a subsequent thermal treatment (650 or 800 °C). The resultant materials were evaluated as self-standing binder-free anodes for LIBs, showing, in the case of the composites formed by SnO₂, very good stability after 400 charge-discharge cycles and reversible capacities per mass of electrode of 1010 and 470 mAh g⁻¹, measured at 50 mA g⁻¹ and 2 A g⁻¹, respectively. Some of

the samples were additionally characterized after 50 charge-discharge cycles to get insight into the possible deactivation process observed for the sample calcined at 800 °C.

Experimental Section

Synthesis of reduced graphene oxide aerogels and Sn-based composites

GO suspension (2 mg mL⁻¹) was prepared according with the procedure previously described elsewhere.^[29] In a first step, graphite oxide was obtained from synthetic graphite provided by Timcal (TIMREX-SFG75) by a modified Hummers method. This method makes use of the Hummers reagents with additional amounts of NaNO₃ and KMnO₄. Briefly, 360 mL of a concentrated H₂SO₄ solution was added into a mixture formed by 7.5 g of synthetic graphite and 7.5 g of NaNO₃. The mixture was then cooled down using an ice bath. Once the mixture was cooled down, 45 g of KMnO₄ was slowly added in small doses to keep the reaction temperature below 20 °C. The solution was then heated up to 35 °C and stirred for 3 h. After this period, 1.5 L of a H₂O₂ (3 % in weight) solution was slowly added, giving rise to a pronounced exothermal effect that increased the temperature up to 98 °C, and the reaction mixture was further stirred for 1h. The remaining solid material was washed with different amount of water and centrifuged again. GO suspension of (2 mg mL⁻¹) was obtained by sonication during 1 h a diluted suspension of graphite oxide, then the suspension was centrifuged (3500 rpm, 30 min), after which any remaining solid was discarded.

For the preparation of the GO aerogels, 100 mL of a graphene oxide suspension (1 mg mL⁻¹) was suddenly freeze in liquid nitrogen and then freeze-dried in a Telstar LyoQuest freeze drier. GO monoliths were then calcined at 650 °C for 1 h under argon atmosphere to obtain the reduced graphene oxide samples (hereafter denoted as rGO). Tin containing samples were synthesized by dissolving 100 mg of SnSO₄ in 100 mL of a GO suspension (1 mg mL⁻¹), then the pH was raised to 9 by the addition of some drops of a 1M NH₃ solution. The mixture was heated at 60 °C for 5 h, and the suspension was then freeze/freeze dried to obtain the macroporous Sn-graphene oxide composites. Sn-reduced graphene oxide aerogels were obtained by the pyrolysis of the aerogels in a horizontal tube furnace. Samples were heated at 1 °C min⁻¹

to 200 °C to avoid the thermal blasting of GO and then to 650 or 800 °C at 2 °C min⁻¹ under dynamic argon atmosphere (100 mL min⁻¹), and maintained at this temperature for 1 h. These samples are hereafter denoted as Sn-rGO-650 and Sn-rGO-800.

Characterization

X-ray diffraction (XRD) patterns were registered for powdered samples in a Bruker D8 X-ray diffractometer; data were collected at 40 kV and 30 mA using CuK α radiation over 2θ within the range from 20 to 70° at steps of 0.02° and residence time of 5 seconds. Raman spectra were recorded with a Renishaw spectrometer (Nanonics multiview 2000) operating with an excitation wave-length of 532 nm. The spectra were acquired with 10 seconds of exposition time of the laser beam to the sample. Scanning electron microscope (SEM) images were acquired in a field emission Quanta 200 FEG microscope from FEI. X-ray photoelectron spectroscopy (XPS) measurements were carried out in the UHV spectrometer chamber with base pressure below 10⁻¹⁰ mbar. The chamber features a hemispherical analyser PHOIBOS 150 with 2D-DLD detector (SPECS) and monochromated X-ray source FOCUS 500 (SPECS) with two anodes: Al K α (hv= 1486.74 eV) and Ag L α (hv= 2984.3 eV).

Electrodes Assembly and Electrochemical Characterization

Electrochemical measurements were carried out in CR2032 type coin cells assembled inside a glove box under argon atmosphere. Half cells were fabricated with the following configuration: Li/separator/rGO samples. Self-standing pellets of 12 mm in diameter and approximately 0.07 mm in thickness, showing densities between 0.10 and 0.15 g cm⁻³ were obtained by punching out a compressed piece of our monolithic materials and used as binder-free working electrodes; lithium metal foil was used as counter/reference and 1.2 M LiPF₆ in ethylene carbonate and dimethyl carbonate 1:1 (v/v) was used as electrolyte.

Cyclic voltammetry (CV) curves were registered in a multichannel potentiostat/galvanostat (Biologic VMP3) at a scan rate of 0.1 mV s⁻¹. Electrochemical Impedance spectroscopy (EIS)

measurements were also carried out in a Biologic VMP3 station within the 100 kHz to 10 mHz frequency range.

Galvanostatic charge and discharge were run in a MACCOR battery tester at different current rates and the specific capacities were calculated per mass of electrode.

Results and discussion

To obtain homogeneous composites formed by GO and tin-based particles, tin sulphate was dissolved in a suspension of GO (1 mg mL^{-1}) in water and the mixture stirred for 24 h. Just few minutes after the addition of the tin precursor, the GO suspension turned from brownish yellow to black, indicating that a partial reduction of the GO sheets had taken place or a certain agglomeration occurred, but at this point no precipitate was detected. Then, pH was increased by the addition of some drops of a 1M ammonia solution to induce the homogeneous precipitation of the tin precursor on the GO layers and to prevent further agglomeration of the graphene sheets.^[30] To assemble the GO sheets and Sn-based particles into a macroscopic macroporous 3D monolithic foam suspensions were first freeze-freeze dried, and then heated under argon atmosphere at 650 or 800 °C to remove part of the functional groups initially present on the GO layers and partially reduce it.

Photographs of a GO-tin precursor foams, prior and after its thermal reduction at 650 °C included in figure 1 (A and B) show the macroscopic view of these self-standing monolithic structures, for which integrity is preserved even after being submitted to thermal reduction treatments. Together with them, other photographs of a film (Fig. 1C) and two electrodes of 12 mm in diameter (Fig. 1D) obtained by physical pressing the Sn-rGO-650 sample evidence the flexible nature of these self-standing films. Figure 1 also includes the SEM images of the three samples (rGO, Sn-rGO-650 and Sn-rGO-800) registered at different magnification. SEM images of rGO aerogel (Fig. 1E and F) show a disordered highly opened macroporous structure formed by thin sheets of rGO. This characteristic macroporous microstructure is produced as consequence of the sublimation of the ice crystals, which are randomly formed by the fast freezing of the suspension in liquid nitrogen. The freeze-drying process did not only allow the

formation of these low dense porous 3D structures, but it also helped to avoid the re-stacking of the layers within the materials. SEM images obtained for the sample Sn-rGO-650 (Fig. 1 G and H) show, in addition to the microstructured rGO layers, the presence of highly homogeneous distribution of particles of approximately 250 nm in diameter attached to or embedded within the graphene sheets.

The sample obtained after calcination at 800 °C (Sn-rGO-800) (I and J images of Fig. 1) still exhibits a highly opened macroporous structure formed by rGO sheets together with Sn-based spherical particles. It is worth noticing that increasing the calcination temperature from 650 to 800 °C gave rise to a significant increase in the size of the Sn-based particles, reaching values of 700 nm in diameter in the case of Sn-rGO-800. The element compositions obtained from the EDX analysis performed on these samples are summarized in table 1. In both Sn-containing aerogels the amounts of tin were quite similar and represent approximately a 37 % in weight of the mass of the composite. The main difference found between the sample calcined at 650 °C to the sample calcined at 800 °C is the lower oxygen content (3.5 % wt. for the Sn-rGO-800 and 8.8 % wt. for the Sn-rGO-650), which can be attributed to a further reduction of the tin oxide particles and the functional groups still present on the GO sheets at the higher temperature.

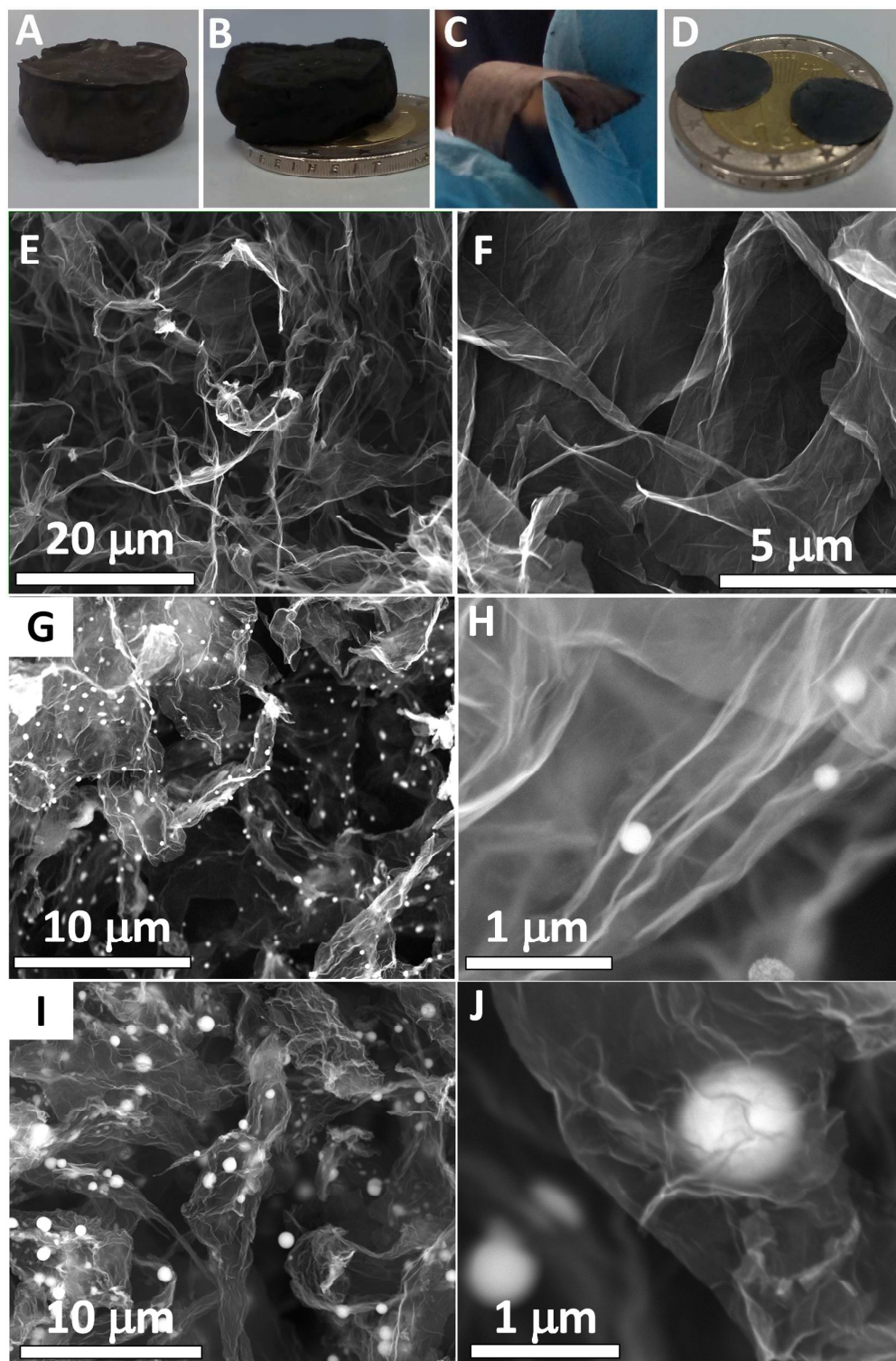


Figure 1. Digital photographs of an aerogel obtained by freeze/freeze drying a 1 mg mL^{-1} suspension of graphene oxide in the presence of the Sn precursor (A), a monolithic Sn-rGO-650 sample (B), a bended film obtained upon pressing the Sn-rGO-650 aerogel (C) and two electrodes of 12 mm in diameter of sample Sn-rGO-650 on top of a 2 € coin (D). SEM images of rGO aerogel (E, F), Sn-rGO-650 (G and H) and Sn-rGO-800 (I and J) samples.

Table 1. Summary of the thermal treatment conditions, composition and crystalline phases of the prepared samples.

	Temperature (°C)	^a C (wt. %)	^a O (wt. %)	^a Sn (wt. %)	^b Crystalline phase	^c I _D /I _G
<i>rGO</i>	650	91.9	7.7	-	rGO	0.9
<i>Sn-rGO-650</i>	650	55.6	8.8	35.8	SnO ₂	1.1
<i>Sn-rGO-800</i>	800	58.0	3.5	38.5	Sn	1.1

^a values measured by EDX analysis; ^b Major crystalline phase determined by XRD; ^c I_D/I_G ratios measured from Raman spectroscopy

The XRD patterns registered for the rGO aerogels, together with those registered for the samples Sn-rGO-650 and Sn-rGO-800 are shown in figure 2. The diffractogram obtained for the rGO aerogel only shows a diffraction peak centred at 26.1° characteristic of the (002) planes from rGO. This broad diffraction indicates a poor ordering of the sheets along the stacking direction, pointing out that the sample comprised only a few graphene layers. XRD pattern registered for the sample Sn-rGO-650 (Fig. 2) also shows three major peaks at 26.5°, 33.8° and 51.7° assigned to the (110), (101) and (211) planes of the SnO₂ (JCPDS card 41-1445) together with other very low intense peaks registered at 30.5, 32.0, 43.9 and 44.9° assigned to metallic tin in a tetragonal phase (JCPDS card 04-0673). It has been previously reported that the complete carbothermal reduction of SnO₂ to metallic tin takes place at 600 °C or even at lower temperature under reductive atmosphere,^[31, 32] however, it seems that in our particular case the functional groups, together with the counterions present on the surface of the graphene sheet could slightly increase the temperature of this process maintaining SnO₂ as the predominant specie within this sample. The XRD pattern registered for the sample calcined at 800 °C (Sn-rGO-800), also plotted in figure 2, clearly shows very sharp and intense peaks at 30.6, 32.1, 43.8 and 45.0°, all of them ascribed to metallic Sn in a tetragonal phase (JCPDS card 04-0673). The Raman spectra (Fig. 2) recorded for the three samples (rGO, Sn-rGO-650 and Sn-rGO-800) show bands at 1350 and 1580 cm⁻¹, which correspond to the disordered (D) and graphitic (G) bands of carbon materials, respectively. The spectra registered for the tin-containing samples exhibit an increase on the D/G intensity ratio with respect to the rGO sample (table 1), which

could be ascribed to a decreasing on the average size of the sp^2 domains and an increasing on the number of those domains probably due to the reaction between Sn precursor and the graphene layers. Two low intense bands at 460 and 620 cm^{-1} were also detected in the Raman spectrum of the sample Sn-rGO-650, which can be assigned to the E_g and A_{1g} active modes of crystalline SnO_2 (inset Fig. 2).^[33]

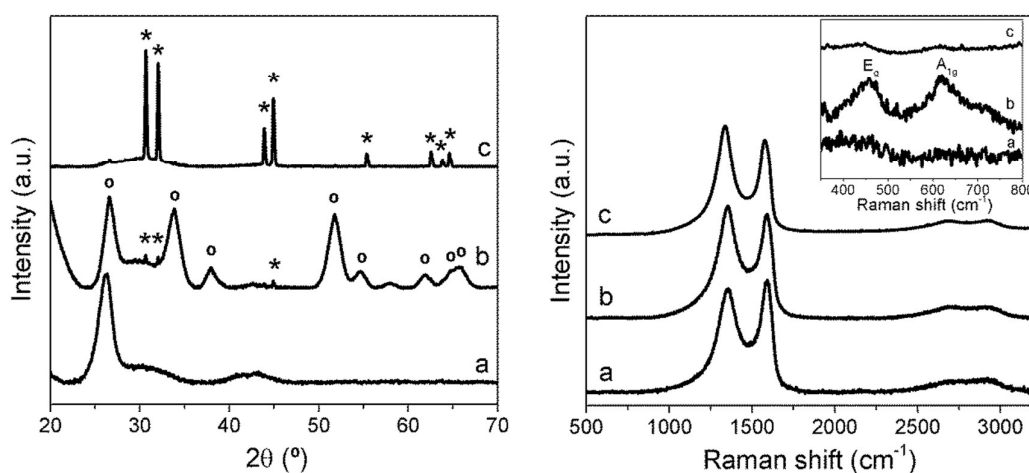


Figure 2. XRD patterns (left figure) and Raman spectra (right figure) registered for samples rGO (a), Sn-rGO-650 (b) and Sn-rGO-800 (c). Peaks assigned to tetragonal metallic Sn and SnO_2 Cassiterite phases are marked with (*) and (°), respectively. Inset shows the enlarged region between 350 and 800 cm^{-1} of the corresponding Raman spectra.

The XPS spectra registered for all these samples (Fig. 3) confirmed the presence of tin species within the Sn-rGO-650 and Sn-rGO-800 samples. The XPS results also supported that the major specie present on the Sn-rGO-650 sample is Sn^{4+} and only a small fraction could be attributed to metallic Sn. In the case of the Sn-rGO-800 sample, the percentage of metallic Sn was significantly higher compared to the sample Sn-rGO-650 (Fig. 3). It is worth to mention that a certain amount of Sn^{4+} was also identified in the sample Sn-rGO-800, which was not detected by XRD. In this case, the presence of Sn^{4+} should be ascribed to a partial oxidation of the tin surface undergone when the sample was exposed to air. The Sn^{4+} amount was easily detected due to the surface-sensitive nature of the XPS technique. The XPS spectra registered for both Sn-containing samples also showed low intense peaks centred at 398.8 eV , which are attributed to the presence of nitrogen incorporated during the synthesis process. The XPS spectrum

registered for the pristine aerogels (rGO) showing only peaks assigned to C1s and O1s is also included in figure 3 for comparison.

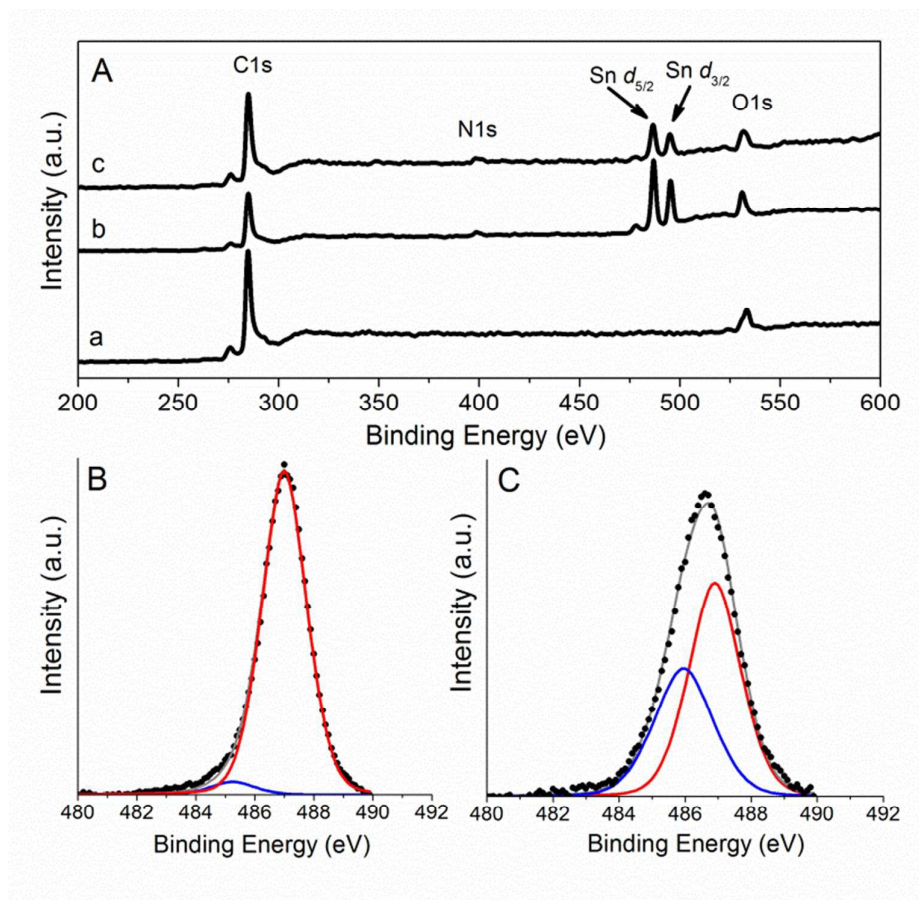
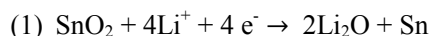


Figure 3. XPS spectra registered for samples rGO (A), Sn-rGO-650 (B) and Sn-rGO-800 (C); and the deconvoluted Sn $d_{5/2}$ peaks registered for Sn-rGO-650 and Sn-rGO-800 samples. Blue line (Sn^0) and red line (Sn^{4+}).

The electrochemical behaviour of tin-containing materials as anodes was firstly evaluated by cyclic voltammetry (CV). The electrodes were prepared, as described above, by pressing and punching out self-standing binder-free electrodes with 12 mm in diameter and approximately 0.07 mm in thickness, namely densities between 0.1 and 0.15 g cm⁻³. These values are higher compared with graphene-based aerogels but still lower than graphite anodes usually obtained at lab scale, which ranged 1.3 g cm⁻³, approximately). Figure 4 shows the first four CV curves registered for the Sn-rGO-650 and Sn-rGO-800 samples in the range between 0.01 and 2.0 V.

Cathodic sweep in the first cycle of the Sn-rGO-650 shows two intense and broad peaks registered at approximately 0.70 and 0.14 V, which are associated with the SnO₂ reduction and SEI formation (equation (1)) and to the alloying process into Li_xSn (equation (2)), respectively. Subsequent cycles (2nd, 3rd and 4th) recorded for this sample show four well defined peaks at 1.49, 0.88, 0.37 and 0.30 V. The peak observed at 0.88 V is associated with the reduction of SnO₂ to Sn, and those peaks registered below 0.37 V can be attributed to the alloying process between Li and Sn to produce the Li_xSn alloy.^[34] The peak that appeared at 1.49 V, which is only observed in the second cycle, could be ascribed to the electrolyte decomposition coupled with the irreversible reduction of functional groups still present on the graphene sheets. The first anodic sweep of Sn-rGO-650 shows four peaks centred at 0.55, 0.65, 0.82 and 1.27 V. Those peaks observed at voltages under 0.90 V have been previously attributed to the lithium dealloying from Li_xSn (equation (2)), while the peak registered at 1.27 V is due to the reversible redox reaction of Sn and SnO₂.^[34] The anodic sweeps of the subsequent cycles are quite similar to the curve registered for the first cycle, and only shows small shifts compared to the pristine ones.



The CV curves registered for sample Sn-rGO-800 (Fig. 4) show in the first cathodic sweep several broad peaks below 1.40 V that are associated, first, to the electrolyte decomposition, SEI formation and at lower voltage to the formation of the Li_xSn alloy. The anodic sweep of the first CV also exhibits very broad peaks at 0.46, 0.70 and 0.82 V attributed to the dealloying of Li_xSn to Sn. The second and subsequent cathodic sweeps are better defined than the first one, and three peaks centred at 0.36, 0.50 and 0.64 V are clearly observed. The peak detected at 0.36 V corresponds to the formation of the Li_xSn alloys, and the other two low intense peaks (0.50 and 0.64 V) are associated with the SEI formation.^[32, 35] In addition to these three peaks, other quite intense one at 1.45 V was also clearly observed in the second cycle curve that it is vanished in

the following cycles. This later peak, which is more pronounced than the one observed in the case of the sample Sn-rGO-650, can be ascribed to the irreversible reduction of some species afforded from the electrolyte decomposition. The anodic sweeps of Sn-rGO-800 show four peaks at ca. 0.46, 0.63, 0.73 and 0.82 V, which have been previously assigned to the transition from the Li_xSn alloy to Sn.^[35-38]

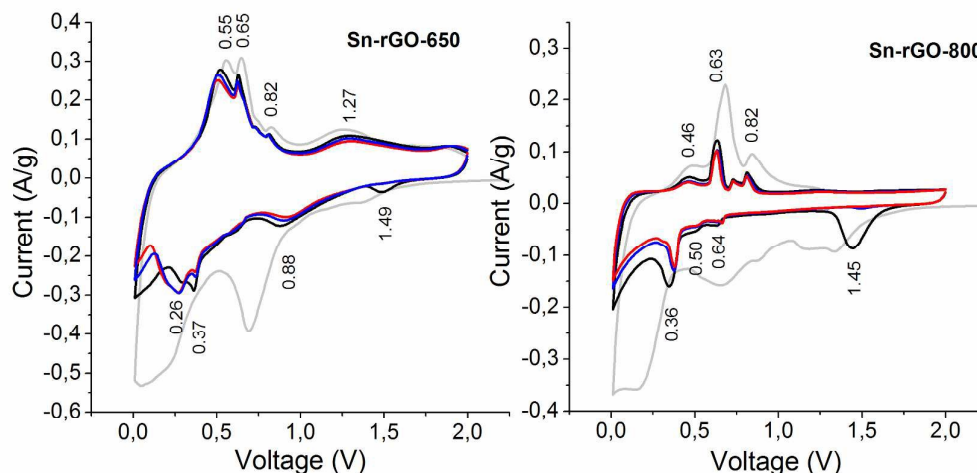


Figure 4. First fourth Cyclic Voltammetry cycles registered for the samples Sn-rGO-650 and Sn-rGO-800. First cycle (gray lines), second cycle (black lines), third cycle (blue lines) and fourth cycle (red lines).

The galvanostatic charge/discharge curves registered for the three samples (rGO, Sn-rGO-650 and Sn-rGO-800) in the first, second and fifth cycles measured at the current density of 50 mA g^{-1} in the potential window of $0.005\text{-}2.0 \text{ V vs Li}^+/\text{Li}$ are depicted in figure 5. Cyclic life and the evolution of the coulombic efficiency with charge/discharge cycles are also shown in figure 5.

In all the cases the specific capacity values were calculated based on the total mass of the electrodes and are summarised in table 2 at different stages of the galvanostatic cycling.

The first cycle of charging process recorded for the tin-free sample (rGO in Fig. 5) shows a very smooth profile with an associated specific capacity of 1154 mAh g^{-1} . This later capacity value strongly decays to 515 mAh g^{-1} during the second charge, showing the irreversible processes that occur during the insertion/extraction of lithium ions such as SEI formation, but the

subsequent reversible capacities were observed to be quite stable over first 50 cycles and capacity of 287 mAh g⁻¹ has been observed at the end of the 50th cycle. The irreversible capacity afforded in the first cycle, which has been previously ascribed to the SEI formation, is favoured on materials with large specific surface areas.

Sn-rGO-650 exhibited a significant overall improvement in comparison with tin-free sample. First charge curve showed a different profile compared with the curve obtained for the Sn-free sample. The first charge branch registered for the Sn-rGO-650 sample shows a plateau around 1.0 V, not observed in the subsequent charge curves, which can be ascribed to the SEI formation. The specific capacity values obtained at this first cycle for the charge and discharge are 1481 and 755 mAh g⁻¹, respectively. Such large capacities are associated to the redox reaction of the SnO₂ along with the alloying/dealloying of the Sn nanoparticles that are formed during the reduction process in addition to the lithium insertion/extraction in the rGO. In the subsequent cycles (2nd to 50th) reversible specific capacities over 611 mAh g⁻¹ were obtained. First charge curve of the Sn-rGO-800 (Fig. 5) also shows a large plateau around 1.0 V similar to the one observed for the Sn-rGO-650 and a specific capacity of 715 mAh g⁻¹ was measured in the former case. In this later case a plateau around 1.6 V is also observed during the first charge that could be attributed to the electrolyte decomposition. The second charge curve shows some steps at 0.8, 0.7 and 0.6 V that were maintained in the subsequent 30 cycles. These small plateaus are in good agreement with the results observed by the cyclic voltammetry, and can be ascribed to the transition from the Li_xSn alloy to metallic Sn. At a certain cycle (30th cycle) these steps are vanished and are not further observed, suggesting that at this point Sn particles do not contribute anymore to the capacity. Similar behaviour has been previously reported by Lou *et al.*^[39] in a system formed by 80 nm Sn particles coated with a carbonaceous shell which claimed that large Sn particles did not have enough space to accommodate volume changes making only possible its reaction at the outer parts of the spheres.

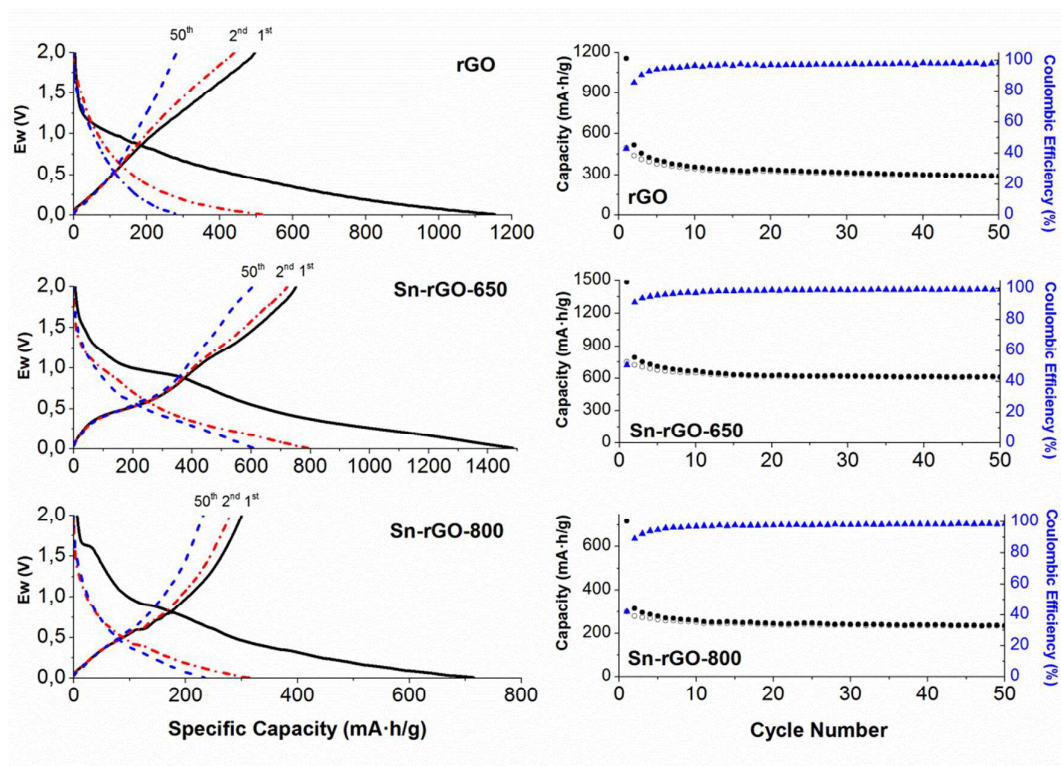


Figure 5. First, second and fiftieth charge and discharge curves registered for the labeled samples (left column). Specific capacities measured from the charge (filled squares) and discharge (empty squares) curves registered at different cycles and its associated coulombic efficiencies (triangles) (right column).

Table 2. Specific capacity values (mAh g⁻¹) calculated from the charge sweep and its associated coulombic efficiencies (in brackets) measured at 50 mA g⁻¹ for the samples at different cycles.

	1 st	2 nd	50 th
<i>rGO</i>	1154 (43%)	515 (85%)	287 (98%)
<i>Sn-rGO-650</i>	1481 (51%)	793 (91%)	611 (99%)
<i>Sn-rGO-800</i>	715 (42%)	314 (89%)	234 (98%)

At this point we wondered what could be the reasons of the differences found in the electrochemical behaviour between the sample Sn-rGO-650 and Sn-rGO-800. In literature it has been previously claimed that small Sn-based nanoparticles can be beneficial to reach high specific capacity values and stability.^[40] However, in the present case both SnO₂ and Sn particles are quite large (~250 and ~700 nm, respectively) compared with most of the Sn-based particle studied as anodes for LIBs.

So, to get insight into the possible causes of the deactivation of sample calcined at 800 °C electrochemical impedance spectroscopy (EIS) measurements of the samples were performed after 50 cycles (figure 6). Nyquist plots of the three samples (Fig. 6A) exhibit a characteristic profile of these sort of composites, which includes a semicircle at the high-medium frequency range in combination with a straight line at the low frequency range.^[41] The charge transfer resistance (R_{ct}) is quite similar in both Sn-containing samples (approximately 100 ohms) and a little bit higher than the R_{ct} measured for the rGO sample (33 ohms). As it can be observed, EIS curves corresponding to the Sn-containing samples did not show great differences between them and appeared almost overlapped, discarding a possible decomposition process that would lead to the deposition of an insulator layer as the main reason why these two samples behaved differently. To further characterise these samples, two coin cells already cycled for 50 cycles were opened and the electrode materials checked on SEM (Fig. 6). The differences observed between both Sn-containing samples are quite clear. While SnO₂ particles were pulverized down into very small nanoparticles produced during its reduction into metallic Sn, those particles that were initially present within the Sn-rGO-800 sample did not show any appreciable change regarding particle size and integrity, being well preserved after 50 charge discharge cycles, and only the formation of a shell around them is observed. It seems that the reaction in such big Sn particles could only proceed at the surface of the spheres or at the outer parts of the spheres avoiding its pulverisation and significantly reducing the specific capacity measured on this sample.

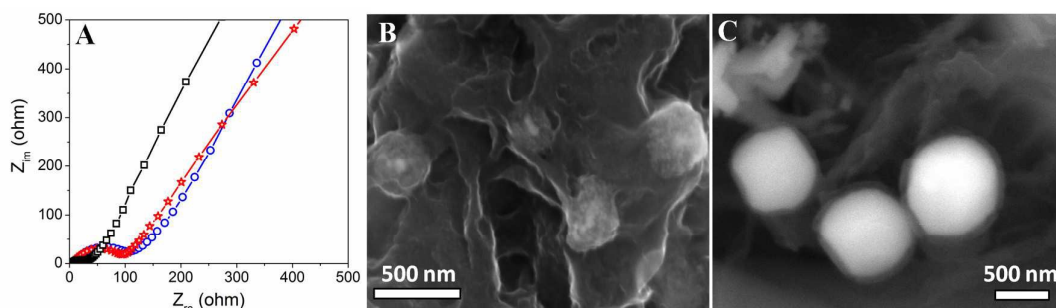


Figure 6. EIS curves registered for rGO (squares), Sn-rGO-650 (stars) and Sn-rGO-800 (circles) recorded after 50 charge-discharge cycles, and SEM images of Sn-rGO-650 (B) and Sn-rGO-800 (C) samples after 50 charge-discharge cycles.

To further evaluate the rate capability and stability of the sample Sn-rGO-650 a new fresh sample with 1.2 mg in mass, 12 mm in diameter and 0.07 mm in thickness (density $\sim 0.15 \text{ g cm}^{-3}$) was prepared and its specific capacity measured at different current rates (Fig. 7). First charge capacity showed a value of 1550 mAh g^{-1} and the reversible capacity measured at 0.05 A g^{-1} is stabilized at 657 mAh g^{-1} . Measurements at 0.1, 0.2, 0.4, 0.6, 0.8 and 1 A g^{-1} showed highly stable capacity values of 627, 615, 566, 512, 440 and 415 mAh g^{-1} , respectively, with associated coulombic efficiencies over 98 %. Once 80 cycles were completed within the voltage window (0.005-2.0 V) the cell was further charged-discharged within the range from 0.005 to 3.0 V to test the behaviour of the material in this voltage window (Fig. 7). Four different rates (0.05, 0.5, 1 and 2 A g^{-1}) were explored within this voltage window, and the capacity calculated at these rates showed average values of 940, 750, 660, 470 mAh g^{-1} , respectively. Once 140 cycles were completed the current rate was restored to 0.05 A g^{-1} showing improved values of specific capacities that reached values of 1010 mAh g^{-1} after 150 cycles, and further highlighting the good performance of this material as anode for LIBs. In Table 3 are summarized some representative values recently reported for composites formed by graphene and SnO_2 . It should be noticed that in all these cases both the specific capacities and current rates are referred to the mass of the active material. It can be observed that when these values are recalculated to the mass of the whole electrode (see table 3), Sn-rGO-650 sample, exhibits comparable or even better performance than composites that make use of conductive carbons to improve their electrical conductivities.

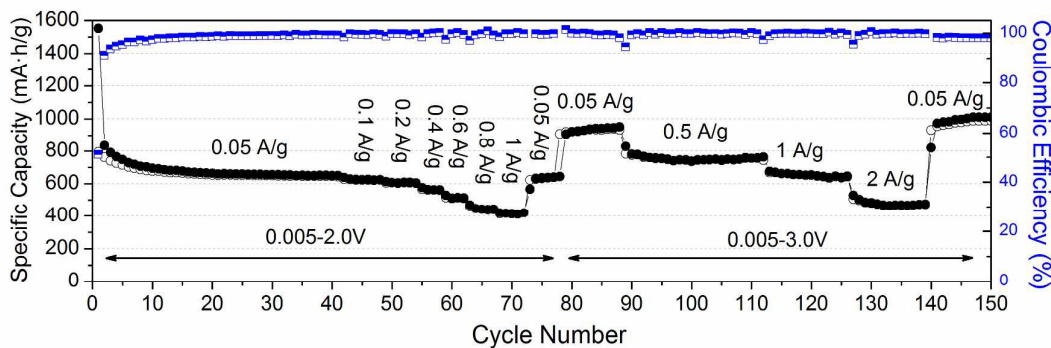


Figure 7. Charge (filled circles) and discharge (empty circles) specific capacities and its associated coulombic efficiencies (bi-color squares) calculated for the Sn-rGO-650 sample along different cycles, measured at different current rates within the 0.005-2.0 V and 0.005-3.0 V voltage windows.

Table 3. Specific capacity values (mAh g^{-1}) measured at different current rates (A g^{-1}) calculated per mass of active material and per mass of electrode recently reported for systems based on SnO_2 and graphene composites.

Reference	Formulation ^a	Capacity ^b (mA h g^{-1})	Current ^b (A g^{-1})	Capacity ^c (mA h g^{-1})	Current ^c (A g^{-1})
42	60:20:20	1100	0.072	660	0.043
		690	3.6	414	2.1
43	80:10:10	1359	0.1	1087	0.08
		1005	0.7	804	0.56
18	80:10:10	1123	0.3	898	0.2
		818	2.0	654	1.6
44	80:10:10	982	0.2	713	0.16
		536	1.6	429	1.3
22	80:10:10	1171	0.2	936	0.16
		700	2.0	560	1.6
45	70:10:20	878	0.1	610	0.07
		519	2.0	363	1.4
This work	100:0:0			1010	0.05
				750	0.5
				660	1.0

(a) active material: conductive carbon: binder in wt. % of the whole electrode; (b) Specific capacities and current rates measured per mass of active material; (c) Specific capacities and current rates calculated per mass of electrode.

The cycling performance of this sample was further tested within the voltage window between 0.005 and 3.0 V at a current rate of 2.0 A g^{-1} . It should be highlighted that after 400 cycles, namely more than 4 months under continuous charge-discharge stages (not shown), the electrode still delivers reversible specific capacities over 350 mAh g^{-1} and associated coulombic efficiencies over 98.5 %, pointing out the stability of this composite and its good performance as anode for LIBs.

Conclusions

Macroporous foams formed by walls of reduced graphene oxide and SnO_2 submicron particles have been prepared by a very simple route, which involves the freeze/freeze drying of a GO suspension in the presence of tin sulphate and its subsequent pyrolysis at $650 \text{ }^\circ\text{C}$ under inert atmosphere. These 3D monolithic structures can be easily compressed to obtain flexible films giving an additional value to the materials. The interpenetrated rGO layers arranged in a 3D

macroporous structure afforded a suitable environment to accommodate the SnO₂ submicron particles providing good mechanical stability and electrical conductivity to the composite and allowing its use without the need of adding any conductive carbon. The performance of this material as binder-free anodes for LIBs showed high stability after 400 cycles and reversible capacities of 1010 and 470 mAh g⁻¹ per mass of electrode measured at 50 mA g⁻¹ and 2 A g⁻¹, respectively.

SEM studies performed for this sample showed that the induced reaction of SnO₂ with Li upon voltage decreasing cause the pulverization to very small of SnO₂ particles, which remains highly active along cycling. An increase on the calcination temperature from 650 °C to 800 °C leads to the complete carbothermal reduction of the SnO₂ particles into metallic Sn with particle size up to 700 nm. As consequence of this particle growing the specific capacity of this later sample is much lower compared to the capacity exhibited by SnO₂-based samples and fades upon cycling mainly due to its large particle size. The complete deactivation of Sn particles occurred after 30 charge-discharge cycles, pointing out that in this particular case the particles size is determinant on its performance as anodes for LIBs. Further studies are under way to test these flexible 3D SnO₂-rGO composites in a full cell configuration.

Acknowledgements

Authors acknowledge E.U. through the Graphene flagship for financial support and thank Dr. A. Bondarchuk for his fruitful help on the XPS data acquisition.

References

- [1] J. M. Tarascon, M. Armand, *Nature*, 2001, **414**, 359
- [2] N. Li, Z. Chen, W. Ren, F. Li, H.-M. Cheng, *PNAS*, 2012, **109**, 17360
- [3] K. Rana, S. D. Kim, J.-H. Ahn, *Nanoscale*, 2015, DOI: 10.1039/c4nr06082b
- [4] C. Wang, Y. Li, Y.-S. Chui, Q.-Hui. Wu, X. Chen, W. Zhang, *Nanoscale*, 2013, **5**, 10599
- [5] Y. Idota, T. Kubota, A. Matsufuji, Y. Maekawa, T. Miyasaka, *Science*, 1997, **276**, 1395
- [6] X. W. Lou, Y. Wang, C. Yuan, J. Y. Lee, L. A. Archer, *Adv. Mater.*, 2006, **18**, 2325

- [7] P. Gurunathan, P. M. Ette, K. Ramesha, *ACS Appl. Mater. Interfaces* 2014, **6**, 16556
- [8] J. S. Chen, X. W. Lou, *Small*, 2013, **9**, 1877
- [9] X. Zhou, W. Liu, X. Yu, Y. Liu, Y. Fang, S. Klankowski, Y. Yang, J. E. Brown, J. Li, *ACS Appl. Mater. Interfaces*, 2014, **6**, 7434
- [10] J. Hassoun, G. Derrien, S. Panero, B. Scrosati, *Adv. Mater.*, 2008, **20**, 3169
- [11] K. S. Novoselov, A. K. Geim, S. V. Morozov, D. Jiang, Y. Zhang, S. V. Dubonos, I. V. Grigorieva, A. A. Firsov, *Science*, 2004, **306**, 666
- [12] J. Yao, X. Shen, B. Wang, H. Liu, G. Wang, *Electrochem. Commun.*, 2009, **11**, 1849
- [13] L.-S. Zhang, L.-Y. Jiang, H.-J. Yan, W. D. Wang, W.-G. Song, Y.-G. Guo, L.-J. Wan, *J. Mater. Chem.*, 2010, **20**, 5462
- [14] S.-M. Paek, E. J. Yoo, I. Honma, *Nano Lett.*, 2009, **9**, 72
- [15] Y. Jiang, T. Yuan, W. Sun, M. Yan, *ACS Appl. Mater. Interfaces*, 2012, **4**, 6216
- [16] S. H. Choi, J.-K. Lee, Y. C. Kang, *Nano Research*, 2015, DOI:10.1007/s12274-014-0646-1
- [17] S. Ding, D. Luan, F. Y. C. Boey, J. S. Chen, X. W. Lou, *Chem. Commun.* 2011, **47**, 7155
- [18] W. Zhou, J. Wang, F. Zhang, S. Liu, J. Wang, D. Yin, L. Wang, *Chem. Commun.*, 2015, **51**, 3660
- [19] D. Cai, T. Yang, B. Liu, D. Wang, Y. Liu, L. Wang, Q. Lia, T. Wang, *J. Mater. Chem. A*, 2014, **2**, 13990
- [20] D. Wang, J. Yang, X. Li, D. Geng, R. Li, M. Cai, T.-K. Sham, X. Sun, *Energy Environ. Sci.*, 2013, **6**, 2900
- [21] B. Chen, H. Qian, J. Xu, L. Qin, Q.-H. Wu, M. Zheng, Q. Dong, *J. Mater. Chem. A*, 2014, **2**, 9345
- [22] Y. Huang, D. Wu, J. Wang, S. Han, H. Lv, F. Zhang, X. Feng, *Small*, 2014, **10**, 2226
- [23] X. Zhou, L.-J. Wan, Y.-G. Guo, *Adv. Mater.*, 2013, **25**, 2152
- [24] Y. Huang, D. Wu, S. Han, S. Li, F. Zhang, X. Feng, *ChemSusChem*, 2013, **6**, 1510
- [25] S. Nardecchia, D. Carriazo, M. L. Ferrer, M. C. Gutiérrez, F. del Monte, *Chem. Soc. Rev.*, 2013, **42**, 794
- [26] B. Wang, W. Al Abdulla, D. Wang, X. S. Zhao, *Energy Environ. Sci.*, 2015, **8**, 869

- [27] G. Zeng, N. Shi, M. Hess, X. Chen, W. Cheng, T. Fan, M. Niederberger, *ACS Nano*, 10.1021/acsnano.5b00576
- [28] S. Han, J. Jiang, Y. Huang, Y. Tang, J. Cao, D. Wu, X. Feng, *Phys.Chem.Chem.Phys.*, 2015, **17**, 1580
- [29] C. Botas, P. Álvarez, C. Blanco, R. Santamaría, M. Granda, P. Ares, F. Rodríguez-Reinoso, R. Menéndez, *Carbon*, 2012, **50**, 275
- [30] D. Li, M. B. Müller, S. Gilje, R. B. Kaner, G. G. Wallace, *Nat. Nanotech.*, 2008, **3**, 101
- [31] X. W. Lou, J. S. Chen, P. Chen and L. A. Archer, *Chem. Mater.*, 2009, **21**, 2868
- [32] X. Zhou, J. Bao, Z. Dai, Y.-G. Guo, *J. Phys. Chem. C*, 2013, **117**, 25367
- [33] X. Zhou, W. Liu, X. Yu, Y. Liu, Y. Fang, S. Klankowski, Y. Yang, J. E. Brown, J. Li, *ACS Appl. Mater. Interfaces*, 2014, **6**, 7434
- [34] X.-T. Chen, K.-X. Wang, Y.-B. Zhai, H.-J. Zhang, X.-Y. Wu, X. Wei, J.-S. Chen, *Dalton Trans.*, 2014, **43**, 3137
- [35] X. Zhou, L.-J. Wan, Y.-G. Guo, *Adv. Mater.*, 2013, **25**, 2152
- [36] W.-M. Zhang, J.-S. Hu, Y.-G. Guo, S.-F. Zheng, L.-S. Zhong, W.-G. Song, L.-J. Wan, *Adv. Mater.*, 2008, **20**, 1160
- [37] D. Deng, J. Y. Lee, *Angew. Chem., Int. Ed.*, 2009, **48**, 1660
- [38] L. Ji, Z. Lin, B. Guo, A. J. Medford, X. Zhang, *Chem. –Eur. J.*, 2010, **16**, 11543
- [39] X. W. Lou, J. S. Chen, P. Chen, L. A. Archer, *Chem. Mater.*, 2009, **21**, 2868
- [40] P. G. Bruce, B. Scrosati, J.-M. Tarascon, *Angew. Chem., Int. Ed.*, 2008, **47**, 2930
- [41] M. Ara, K. Wadumesthrige, T. Meng, S. O. Salley, K. Y. Simon Ng, *RSC Adv.*, 2014, **4**, 20540
- [42] S. Nam, S. J. Yang, S. Lee, J. Kim, J. Kang, J. Y. Oh, C. R. Park, T. Moon, K. T. Lee, B. Park, *Carbon*, 2015, **85**, 289
- [43] L. Liu, M. An, P. Yang, J. Zhang, *Sci. Rep.*, 2015, **5**, 9055
- [44] S. Li, W. Xie, S. Wang, X. Jiang, S. Peng, D. He, *J. Mater. Chem. A*, 2014, **2**, 17139
- [45] S.J.R. Prabakar, Y.-H. Hwang, E.-G. Bae, S. Shim, D. Kim, M. S. Lah, K.-S. Sohn, M. Pyo, *Adv. Mater.* 2013, **25**, 3307